

Effect of WC Nano-powder on Properties of Plasma Electrolytic Oxidation coating Fabricated on AZ31B Alloy

H. Nasiri Vatan, R. Ebrahimi-Kahrizsangi*, M. Kasiri Asgarani

Advanced Materials Research Center, Materials Engineering Department, Najafabad Branch, Islamic Azad University, Najafabad, Isfahan, Iran

*E-mail: rezaebrahimi@iaun.ac.ir

Received: 26 October 2015 / Accepted: 4 December 2015 / Published: 1 January 2016

AZ31B Mg alloy substrate was coated in aqueous sodium aluminate, sodium silicate and KOH electrolyte using PEO method in different processing times with and without WC nano-powders. Thickness, composition, morphology and hardness examined using eddy current, EDS, SEM and micro-Vickers hardness tester respectively. Electrochemical corrosion tests were carried out using potentiodynamic polarization technique. Pin on disk wear test was implemented in order to investigate effect of added WC nano-powders in nano-composite ceramic coating on AZ31B alloy. In cross section investigation, increase in thickness with coating time and in coating surfaces increase in porosity percentage and mean pore diameter with coating time was revealed. In presence of nano-powders wear rate, wear track width was decreased and roughness and COF increased. Results showed that presence of nano-powders can modify the composition of coating and subsequently corrosion resistance of coated samples. Also Hardness of nanocomposite coating is about 1.62 times greater than that of ordinary coatings.

Keywords: PEO; Nano-composite coating; WC; Mg AZ31B

1. INTRODUCTION

Tungsten Carbide (WC) is extensively used in hard, wear resistant coatings as a result of its thermal stability, oxidation and wear resistance at high temperatures [1]. Recently a promising surface treatment method, named Plasma Electrolytic Oxidation (PEO), capable of protecting valve metals and their alloys against wear and corrosion, has been developed and is used for Magnesium based alloys. Among surface treatment methods studied on Mg alloys, PEO is one of major interests. PEO has developed under conventional oxidation processes category, an effective method to improve wear and corrosion resistance of Mg alloys [2].

PEO is introduced as most commodious and most effective surface modification method designed to produce a ceramic coating on metals and alloys in proper electrolyte. Surface properties of PEO coatings like, wear resistance, corrosion resistance, thermal resistance and adhesion to substrate could be significantly improved. Conventionally a silicate based electrolyte is used and PEO coatings on Mg are mostly consisted of MgO and Mg₂SiO₄, which can improve wear resistance of Mg alloys [3].

Plasma Electrolytic Oxidation (PEO) which sometimes is called Micro Arc Oxidation (MAO) or Spark anodizing, is a promising surface treatment for Al and Mg alloys in replacing Cr(VI) for corrosion protection and tribological properties [4]. PEO technology is successfully used for producing ceramic coatings on Al, Mg and Ti, and corrosion properties of treated Mg alloys generally depend on process parameters and chemical composition of substrate and electrolyte.

Nano-composite ceramic coatings of WC are potentially useful in improving surface wear resistance and exhibit perfect corrosion resistance. Some deposition techniques such as arc-discharge plasma, gas-flame spray [5], vacuum deposition methods, high temperature glass annealing and laser surface modification [6] are used to produce nano-composite ceramic coatings on metal surfaces. These methods require high substrate temperatures in order to achieve sufficient adhesion to substrate through high contact forces [5]. Recent studies show that nano-composite coatings exhibit interesting combinations of wear and corrosion resistance with mechanical strength, surface adhesion and thermal properties. This specially applies to Mg and its alloys in aerospace and automotive applications [7].

Several studies signify that PEO coating quality depends on technical parameters such as current density, electrolyte composition and temperature and so on. It has been reported that higher current densities and lower temperatures are beneficial for coating growth. Ma et al Stated that oxide film grown in silicate electrolytes possess high wear resistance, while films from phosphate base electrolytes show superior corrosion resistance [8]. They also reported that adding NaAlO₂ to electrolyte enriches coating from MgAl₂O₄ [9]. Duan et al studied effect of phosphate, borate and fluoride additives on coating efficiency of Mg alloys. They realized that oxide films in both borate and fluoride have better corrosion resistances [10].

Any way studies are focused on properties, function and morphology evaluations of composite coatings. Formation kinetics, changes in morphology of surface and composition of nano-composite coatings with time, current density and temperature has not been studied thoroughly yet. In this way, aim of this study is to achieve nano-composite coatings by PEO process. Electrolyte composition has been selected with desired properties in mind. For example dilute alkaline electrolytes with considerable concentrations of sodium silicate for maximum growth rate and nano-composite coating thickness are utilized. Although it has stated generally that sodium silicate increases growth rate, but few works have studied it quantitatively. Most studies stated that thick coatings with high corrosion resistance can form under low temperature and in specific electrolyte conditions. High concentration of sodium silicate in electrolyte leads to higher growth rates probably due to more silicate deposition while substrate oxidation. Moreover, addition of sodium silicate and alkalinity of electrolyte decrease oxide dissolution and increases growth rate. Owing to significant role of coating time, this study is an attempt to investigate time coating parameter of PEO process and presence of WC nano-powders on characterization, electrochemical corrosion behavior, morphology and composition of WC nano-

composite PEO coatings.

2. EXPERIMENTAL

Samples used in this study were AZ31B prepared as sheets with 2 mm thickness acquired from Bohler with $30 \times 30 \text{ mm}^2$, relative composition of samples is presented in Table 1.

Table 1. Composition of AZ31B alloy used in this study.

element	Mg	Zn	Si	Mn	Fe	Cu	Ni	Al
Wt%	Balance	0.6-1.4	Max 0.1	0.2	Max 0.005	Max 0.05	Max 0.005	2.5-3.5

Samples were cut into rectangular shape from the sheet and sample preparation included grinding with abrasive SiC papers in 5 different meshes including 200, 800, 1200, 2500 and 4000. Deionized water was used to wash and hot air flow was used to dry samples. In order to achieve electrical contact, samples were drilled and screwed from smallest surface to serve as anode.

Electrolyte composition used in PEO process was based on 2 gr/L NaAlO_2 , 2 gr/L Na_2SiO_3 and 0.5 gr/L KOH concentrations and WC nano-powders manufactured by US Research Nanomaterials, Inc. (US Nano) with dimensions less than 80 nm (Presented in Fig. 1) was added in 5 gr/L concentration to electrolyte. Philips CM 120 TEM was implemented to determine nanoparticle sizes. A&D-GR202 balance with ± 50 micro gram accuracy was used for weighting. Suspension of nanoparticles was stirred for 6 hours on magnetic stirrer in order to achieve a uniform distribution of nanoparticles.

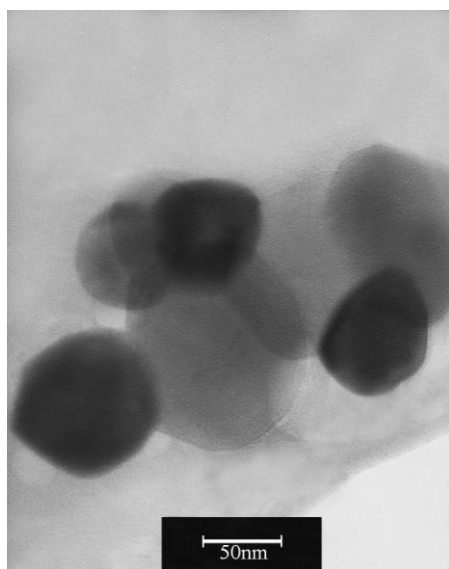


Figure 1. TEM image of WC nano-powders used to fabricate nanocomposite.

PEO station included a 20 KW power supply, a current rectifier with maximum voltage of 600 V and electrolyte cooling system which maintained temperatures below 30 degrees Celsius. During process of coating, applied current density was equal to 23.1 mA/cm². Coating time was 5, 10, 15 and 20 minutes. After coating process, samples were brought out, washed with distilled water and dried in warm air flow (Table 2).

Table 2. Process conditions of PEO coated samples.

Sample Code	Nano-powder	Time of Coating (min)
NP5	WC	5
NP10	WC	10
NP15	WC	15
NP20	WC	20
SS5	—	5
SS10	—	10
SS15	—	15
SS20	—	20

In order to study the morphology of surface, cross section and composition of coatings, WEGA TESCAN SEM with RONTEC EDS analyzer and ZEISS SIGMA/VP SEM were used. Before cross section studies, samples were cut using coping saw and then mounted in resin, grid and polished. Image-J software was used to analyze SEM micrographs to calculate percentage of porosity, pore dimension and coating thickness. According to ASTM G-3 standard, corrosion test was carried out by using EG&G-A273 Potentiostat/Galvanostat in a standard flat cell. An area of coatings equal to 0.196 cm² was exposed to 3.5 %wt NaCl electrolyte, platinum grid was used as counter electrode and SCE as reference electrode. All samples were in contact with electrolyte for 30 min in order to achieve stability. Polarization test was carried out from -300 mV to 700 mV vs. OCP with 1 mV/s scan rate. Softcorr III software and PARCalc analysis was implemented to extract relevant data. Surface roughness (R_a) of coatings was evaluated using Taylor Hobson Sutronic25, Stylus type surface profilometer with ± 10 nm accuracy. In order to study wear resistance and coefficient of friction of samples pin on disk wear test was performed according to ASTM G-99 standard. In order to determine coating thickness QnIX8500 instrument was implemented.

3. RESULTS AND DISCUSSION

During coating formation associated with sparking phenomena occurring between electrolyte and anode (sample), in order to keep current density constant, potential between anode and cathode (water cooling stainless steel) altered and variations of potential were measured by connecting the anode and cathode to voltmeter linked with a computer. Fig. 2 illustrates changes of potential versus time during coating process for samples coated for 20 minutes. Since samples coated in less coating

times have similar results to illustrated curve, just results of samples coated in longest time, with and without WC nano-powders have been reported here. Results are in agreement with those reported by other authors [11] in similar studies and it can be observed that sample coated in suspension without nano-powder shows 10 to 15 V higher sparking potentials compared to sample with nano-powders, in other words owing to same current density for both types of samples, the amount of energy required for creating PEO coating, in case of presence of nano-powders is lower than that without nano-powders. This can be attributed to less porosity resulted from presence of nano-powders in coating and consequently less resistivity of coating [12]. At initial stages of sparking, layer resistance is considerably higher compared to later stages, so that more potential input is needed to keep current density be constant. But after approximately 100 s, increasing rate of coating resistance is dropped and corresponds with thickness of coating. This phenomenon is probably due to double layer structure of PEO coating on Mg alloys in which initial thin layer, inner layer, has compact structure accordingly much more resistance than thick outer layer that has porous structure and less resistance [13]. Also it can be observed that slope of both diagrams is almost equal and relates to rate of increase of coating thickness.

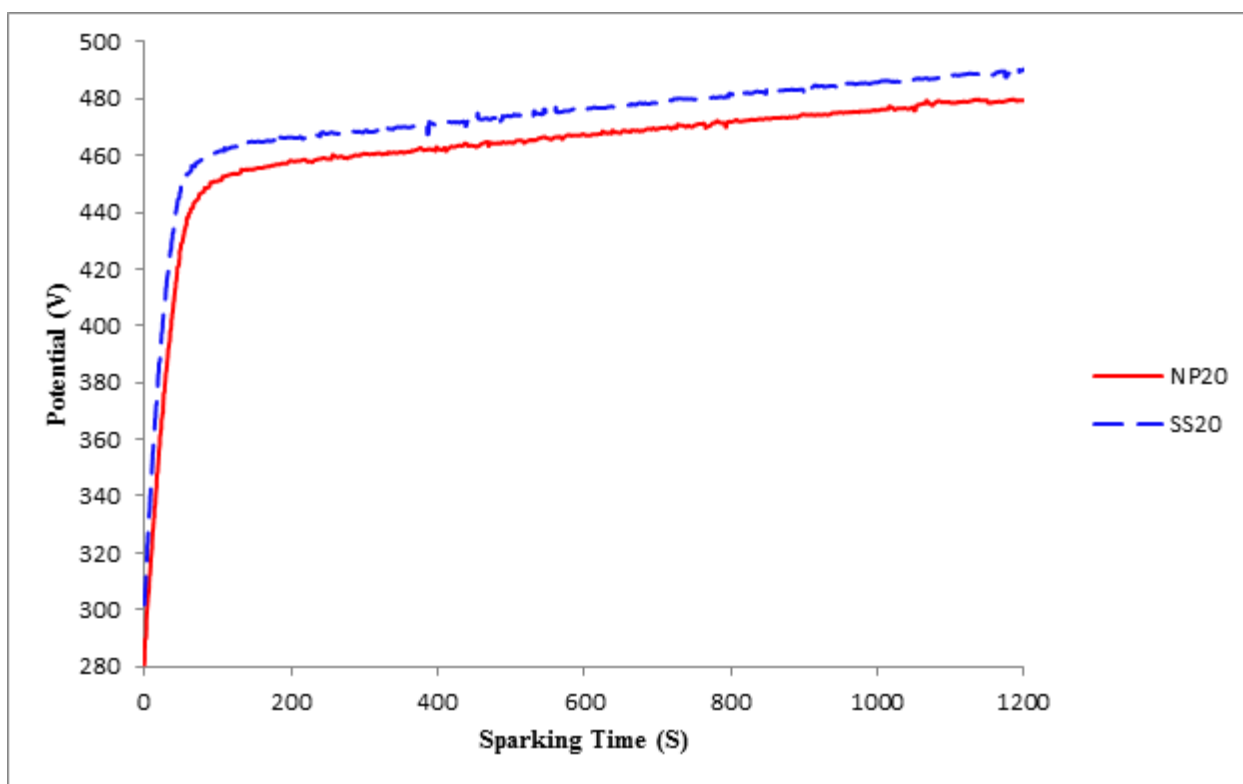


Figure 2. Potential variations vs sparking time during coating process for samples coated for 20 min. Increase of potential is due to keep current density constant. The sparking time is almost the same coating time.

Fig. 3 shows SEM images of coatings' free surfaces. Comparing the samples containing nano-powders with their counterparts without nano-powder, it can be observed that area fraction of porosity in nanocomposite coatings (coatings containing nano-powders) is lower than that in normal coating,

the fact that is consistent with reports of other studies [12, 14, 15]. Furthermore by increasing of coating time, because of growing up the size of sparks, topmost structure of coating become coarse gradually for both types of coatings. Table 3 presents weight variation of samples during coating process, thickness of coatings, porosity and mean diameter of pores existing on free surface of coatings. It can be seen that all samples have positive weight change implying that net growth of PEO coatings is outward and rate of fabrication of coating is higher than rate of consuming of substrate. Also weight gain of all coatings, increases by coating time. As expected, by increase of coating time and consequently increase of size of last sparks, mean diameter of top surface pores and area fraction of porosity increase by coating time. This results match other findings in nano-composite coatings with PEO process [16]. As indicated by results in table 3, thickness of coatings containing nano-powders is generally more than that of coatings without nano-powder [15]. In addition, thickness of both types of coatings, increase by coating time. Besides, coating thickness measured by probe for all samples is higher than that measured by analysis of SEM images [17].

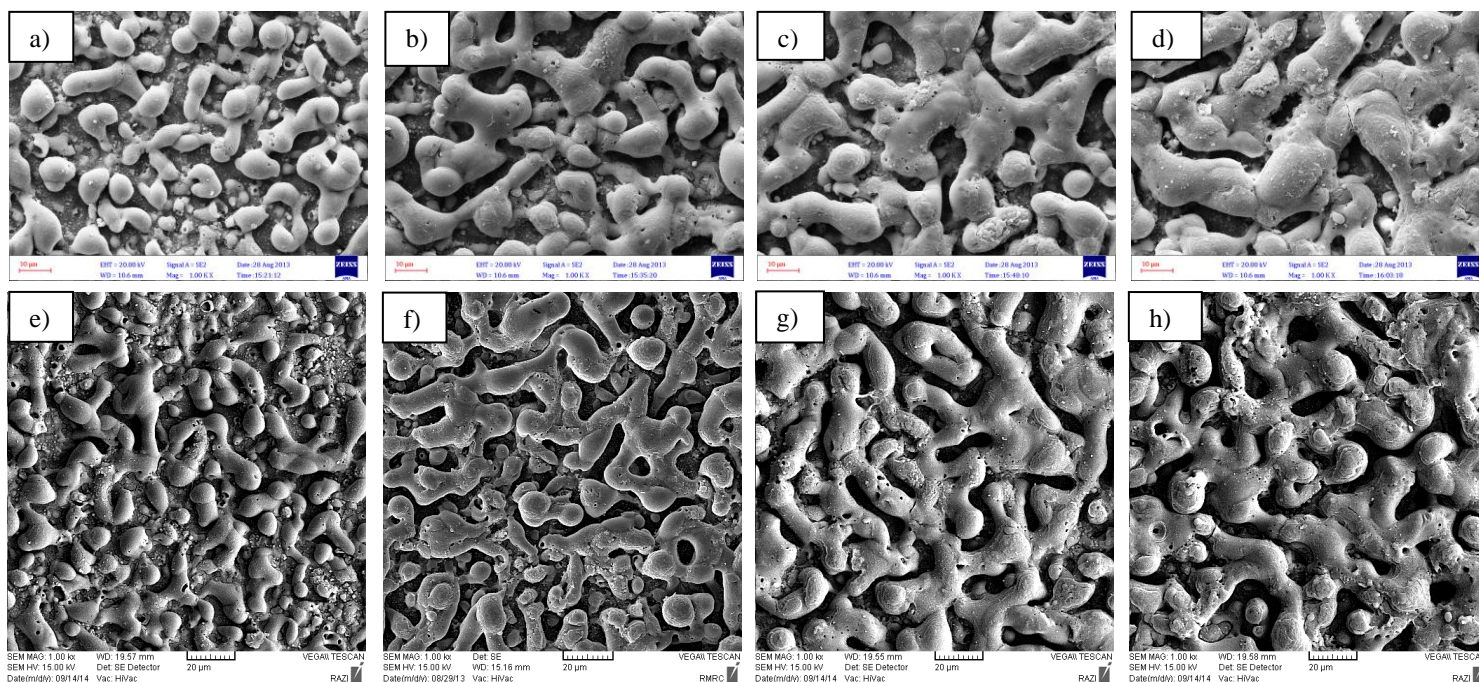


Figure 3. SEM images of free surface of coatings: a) NP5, b)NP10, c)NP15, d)NP20, e)SS5, f)SS10, g)SS15, h)SS20. First row images correspond to nanocomposite coatings and second row ones correspond to normal coatings. From left to right, the pancake-like structures become coarser by coating time in both types of coatings.

Table 3. Weight, porosity, thickness and mean pore diameter of coatings.

Sample code	Weight before PEO (g)	Weight after PEO (g)	Weight variation %	Average of hole diameter (μm)	Surface Porosity (%)	Probe thickness (μm)	Cross thickness (μm)	Probe thickness / Cross thickness
NP5	4.11639	4.12646	0.24463	3.95	7.14	12.89	6.77	1.90
NP10	4.26705	4.28242	0.36020	5.55	14.65	16.13	7.00	2.30

NP15	4.67392	4.69409	0.43154	7.42	14.78	18.51	7.34	2.52
NP20	4.47000	4.49293	0.51297	9.34	14.83	20.69	9.60	2.16
SS5	5.22239	5.23423	0.22672	6.32	15.55	12.99	4.06	3.20
SS10	3.55093	3.56295	0.33850	8.12	18.17	15.99	4.48	3.57
SS15	5.10653	5.13181	0.49505	9.27	19.29	18.23	4.81	3.79
SS20	5.12214	5.15236	0.58999	10.22	22.17	20.03	12.99	1.54

Fig. 4 shows surface images and corresponding element distribution for samples containing nano-powders. Uniform distribution of all elements is evident in images. Since detection of carbon element by EDS method is associated with great error, therefore in order to discover existence of WC nano-powders in coatings, detecting of tungsten element as behalf of WC nano-powders was performed. On the other hand, reports of other studies carried out by XRD analysis, show that nanoparticles added to structure of PEO coating, are remained stable during fabrication of coating [18, 19].

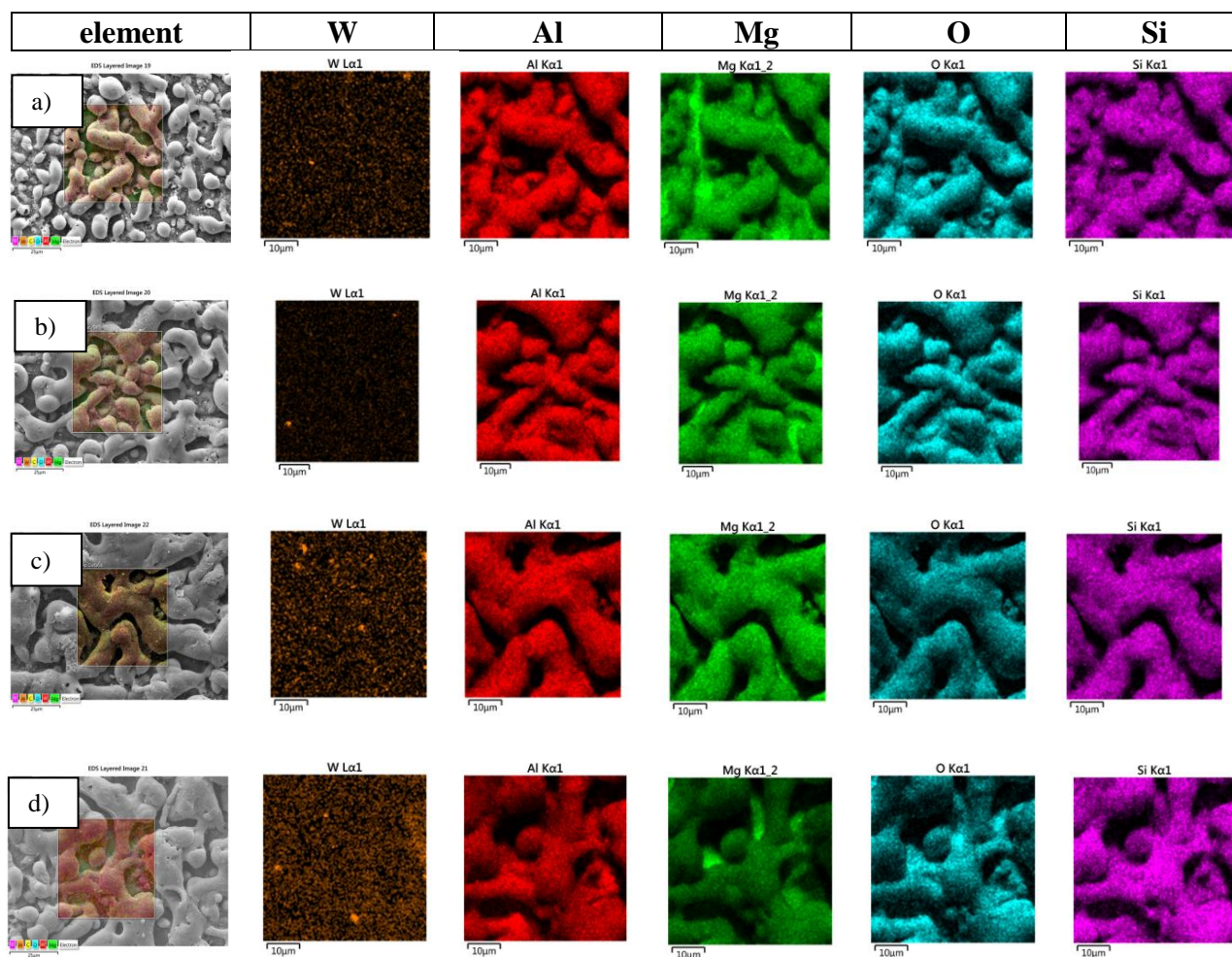


Figure 4. W, Al, Mg, O and Si element distribution map obtained from EDS analysis from free surface of nanocomposite coatings: a) NP5. b) NP10. c) NP15. d) NP20.

Table 4. EDS, elemental fraction results of coating surfaces.

Sample code	W (wt%)	Si (wt%)	O (wt%)	Mg (wt%)	Al (wt%)
NP5	0.99	12.10	33.11	34.87	18.92
NP10	1.01	14.41	31.73	32.85	20.00
NP15	1.95	15.84	29.16	32.38	20.67
NP20	2.68	14.92	28.55	31.59	22.26
SS5	—	18.92	34.48	34.12	12.48
SS10	—	21.10	33.02	32.89	12.99
SS15	—	22.85	31.76	32.66	12.73
SS20	—	25.01	29.51	30.28	15.20

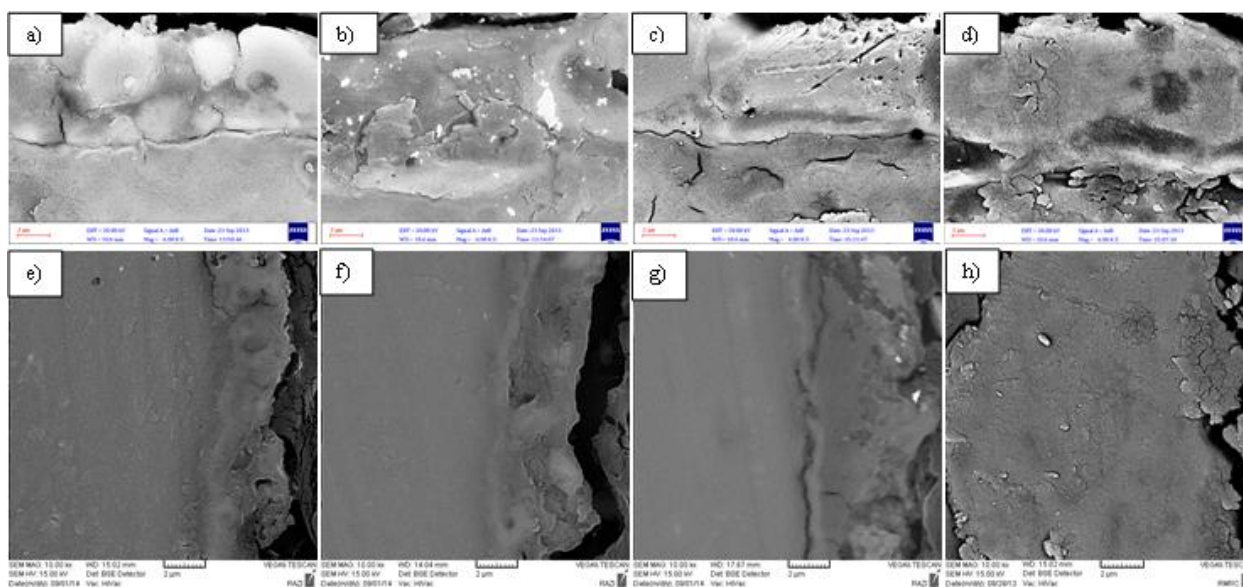


Figure 5. SEM images from cross section of coatings: a) NP5, b)NP10, c)NP15, d)NP20, e)SS5, f)SS10, g)SS15, h)SS20. First row images correspond to nanocomposite coatings and second row ones correspond to normal coatings. From left to right side, the coating time is increased.

Table 4 presents EDS results of coating surfaces, showing increase in nano-powder absorption with time in samples containing nano-powders. It should be noted that only small portion of %Al is originated from composition of substrate and the rest is originated from electrolyte. Tungsten was introduced into coatings from 0.99%, minimum value, for sample NP5 to 2.68%, maximum value, for NP20 sample without any visible agglomeration. An important result should be pointed out is that rate of embedding of nano-powders into coatings is gradually increasing by coating time, so that amount of nano-powders embedded into sample coated for 20 min is much more than that embedded into sample coated for 5 min; this from one side can be due to growth of spark size providing bigger pores for infiltration of nano-powders and from other side can be due to contribution of initial dense layer to less absorption of nano-powders. According results represented in table 4, it can be implied that absorption of WC nano-powder can lead to change composition of coatings such that in presence of nano-powders, formation of magnesium aluminate phase is facilitated.

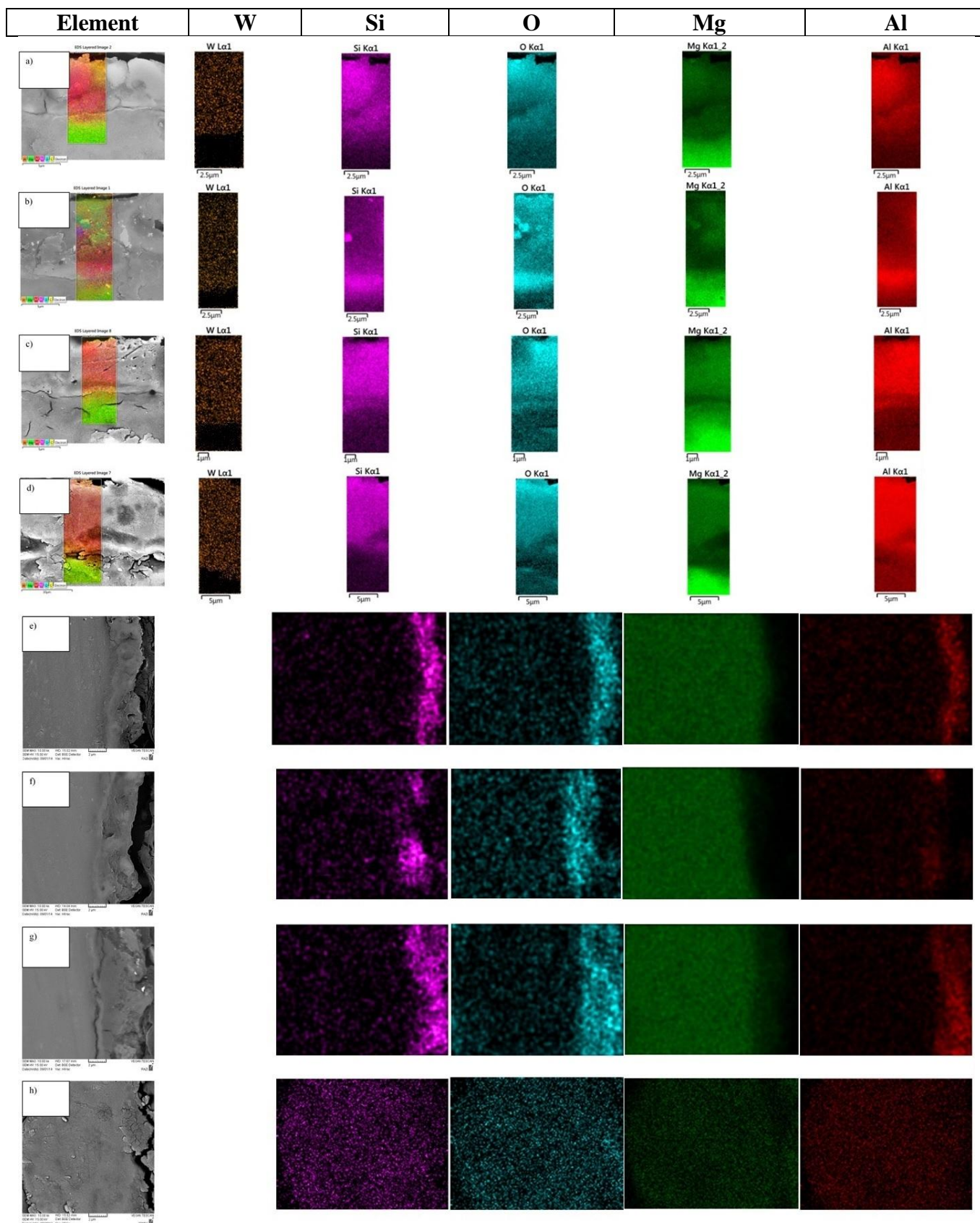


Figure 6. W, Al, Mg, O and Si element distribution map obtained from EDS analysis from cross section of coatings: a) NP5, b)NP10, c)NP15, d)NP20, e)SS5, f)SS10, g)SS15, h)SS20. For normal coatings, W element detection was not performed.

This might be due to greater voltage (energy) generated for samples without nano-powder (Fig. 2) anticipated formation of magnesium silicate phase [20, 21]. Stojadinović et al [18] found out PEO process time affects on composition of formed coating. This case also can be seen that by increase of coating time for both types of coatings, amounts of O and Mg in the coating decrease, indicating that more reactions between MgO and silicate and aluminate ions take place leading to formation more amounts of magnesium silicate and magnesium aluminate.

In order to investigate coatings for more details, cross section SEM images of coatings are presented in fig. 5. Mean thickness measured from images are listed in Table 3, once again showing thickness increase with coating time as well as inner thin compact layer of coating.

The difference between thicknesses acquired from probe and measured from cross section images, 1.5 to 3.5 times more value from probe, is due to porosity and uneven surface. Addition of nano-powders seems to increase coating compactness, matching other findings in similar studies [22]. It seems that adhesion of coatings without nano-powder to substrate is higher than that of coating containing nano-powders, this fact can be realized from less cracks elongated through coating/substrate interface for samples without nano-powder. Furthermore presence of numerous cracks in coating structure can be originated from ceramic nature of coatings undergone quench process through formation at elevated temperature of discharge tunnels and rapid cooling to room temperature of electrolyte.

Fig. 6 shows EDS map of elements distributed across the coatings and as it can be seen, elements including W, distributed uniformly in coatings and from early stages of coating formation, embedding of nano-powders into coating layer initiates. Besides, infiltration of somewhat W beyond the coating/substrate interface, i.e. into substrate, implies the partially destructive effect of sparks which by piercing can lead to entering of nano-powders in substrate. It is proved that in addition to MgO phase commonly presented in all PEO coatings, other phases such as MgAl_2O_4 and MgSiO_4 can be generated from reaction between substrate and SiO_4^{2-} and AlO_2^- species in electrolyte [23]. According to Fig. 6 and table 4, it can be found out that in presence of nano-powders, formation of aluminate phase in coating is preferable, and about samples without nano-powder, formation of silicate phase is preferable.

Fig. 7 contains potentiodynamic polarization curves of coatings. Owing to presence of Cl^- anion in corrosion medium, pitting corrosion is dominant mechanism of corrosion [24], accordingly samples with nano-powders show slightly better behavior compared to those without nano-powder caused by pore closure. Furthermore passive region can be seen for all samples which can be attributed to formation of inner dense layer in all coating. In respect of samples containing nano-powders, by increase of coating time, no appreciable changes in corrosion resistance can be seen; this can be due to filling of pores by means of nano-powders for all nanocomposite coatings retarding equally penetration of Cl^- ions. About coatings without nano-powders by increase of coating time, probably due to thickening of coatings, corrosion behavior is totally improved and diagrams shifted to up and left, more noble potential and less corrosion current density, respectively. Since presence of nano-powders can change the chemical composition of coating and MgAl_2O_4 can form more, therefore improvement of corrosion resistance of nano-composite coatings can be attributed to their different chemical compositions. Similar results in which composition of coating improves the corrosion resistance can be

addressed at work of Zhang et al. [25]. The corrosion parameters derived from polarization curves are presented in table 5. These data are calculated by Softcorr III software. As expected, regarding to i_{corr} addition of WC nano-powders to coatings, doesn't improve corrosion behavior significantly and generally increase of coating thickness has more effective contribution in decreasing corrosion current density. Greatest i_{corr} is for sample SS5 with lowest thickness (table 3) and without nano-powders; moreover its corrosion potential represents most active behavior of this sample. Another point which can be found is more cathodic tafel slopes of nanocomposite coatings compared to normal ones that can be attributed to more susceptibility to become polarized due to either concentration or resistance. In other words, presence of nano-powders can retard the migration of species in cathodic reaction of coated samples.

Fig. 8 depicts changes in coefficient of friction (COF) during wear test of samples with and without nano-powders, and Table 5 shows wear rate, hardness, wear track width, roughness and COF. Nano-powder presence has increased coating strength and decreased wear rate. Additionally with nano-powder introduction into coatings, coatings are roughened slightly, which seems to have no effects on wear rate results.

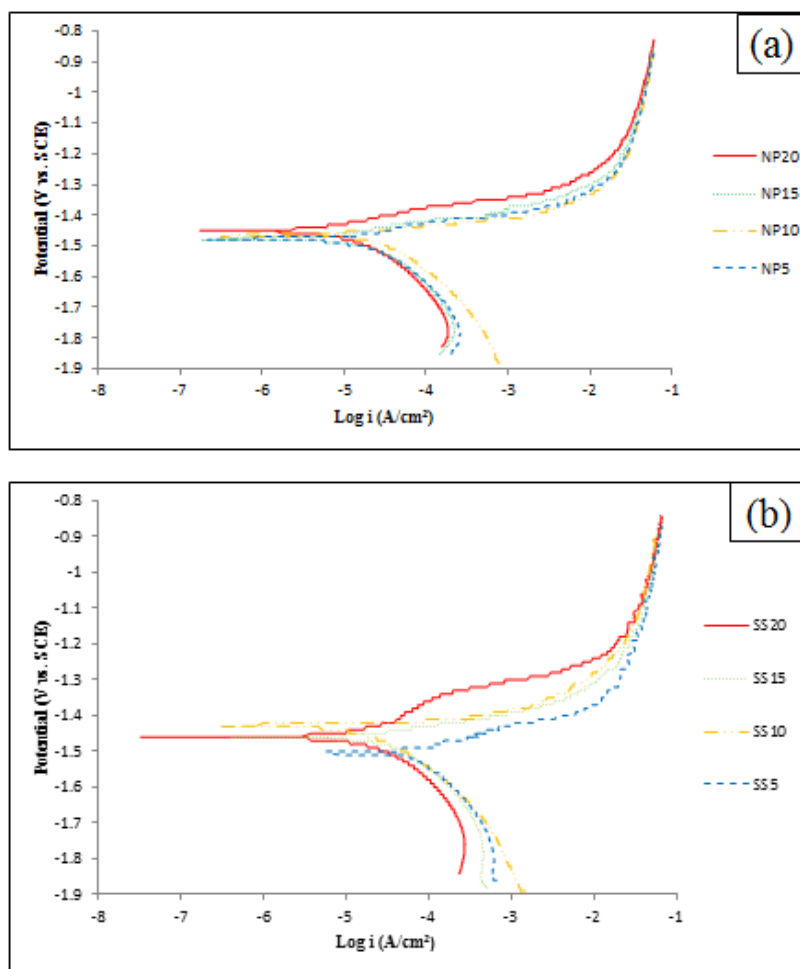


Figure 7. Potentiodynamic polarization curves (potential vs. log current density) of samples obtained from corrosion test in 3.5 %wt NaCl electrolyte: a) samples with and b) without WC nano-powders. The data in table 5 are extracted from these curves.

Table 5. Corrosion parameters derived from polarization curves in Fig. 7.

Sample code	$\beta_a \times 10^{-3}$ (V/decade)	$\beta_c \times 10^{-3}$ (V/decade)	E_{corr} (V vs. SCE)	i_{corr} ($\mu\text{A}/\text{cm}^2$)
NP5	71.99	182.40	-1.478	17.94
NP10	66.10	185.60	-1.466	24.79
NP15	116.10	174.40	-1.477	19.72
NP20	93.08	156.60	-1.451	10.23
SS5	69.14	320.80	-1.505	102.60
SS10	122.20	167.40	-1.427	20.08
SS15	67.54	200.00	-1.462	37.31
SS20	188.20	223.20	-1.460	31.85

Wear and corrosion tests, show that even in short times of coating in presence of nano-powder, satisfy corrosion and wear resistance demands, although NP15 sample has highest hardness. Average COF of coatings containing nano-powders is more than that of ordinary coatings, and this is a shortcoming because can lead to more friction and wear when coated sample contacts with other parts, however comparing wear track width and average rate of wear in both types of coatings, the positive contribution of nano-powders in improvement of tribological properties can be implied, the fact that is in agreement of other authors' results [26]. Also it can be observed that, friction behavior of nanocomposite samples is very similar, while that of ordinary samples have very different wear behavior, likely because of more uniformity of nanocomposite coatings and non-uniformly distribution of pores in ordinary coatings.

As Liu et al. [27] have reported, this trend of COF variation in which there is great fluctuation in early stages of wear test followed by relatively gently oscillation, can be attributed to composition changes through the thickness, so that inner layers of coatings mainly comprise from MgO phase and therefore have less fluctuations in COF vs. distance. Another important result is that generally by increase of coating time, wear rate increases which can be explained such that by increase of coating time, last layers of coatings are formed more loose and porous and consequently will be worn more easily. Average hardness of coatings containing nano-powders 1.62 times higher that of ordinary coatings indicating proper cohesion of nano-powders in the structure of coatings.

As shown in table 6, addition of nano-powders to coatings leads to increase of roughness. Roughness of free surface of coatings is mostly originated from alternatively protuberances and holes of pancakes [28, 29]. The holes in fact are discharge tunnels in where melting and reaction of materials take place, nevertheless it can be concluded that during solidification of melted and reacted materials, nano-powders act as nucleator and causes attraction and concentration of materials surrounding of themselves and consequently vacating of aperture of hole from materials finally leads to more and greater protuberances and holes in surface of coating.

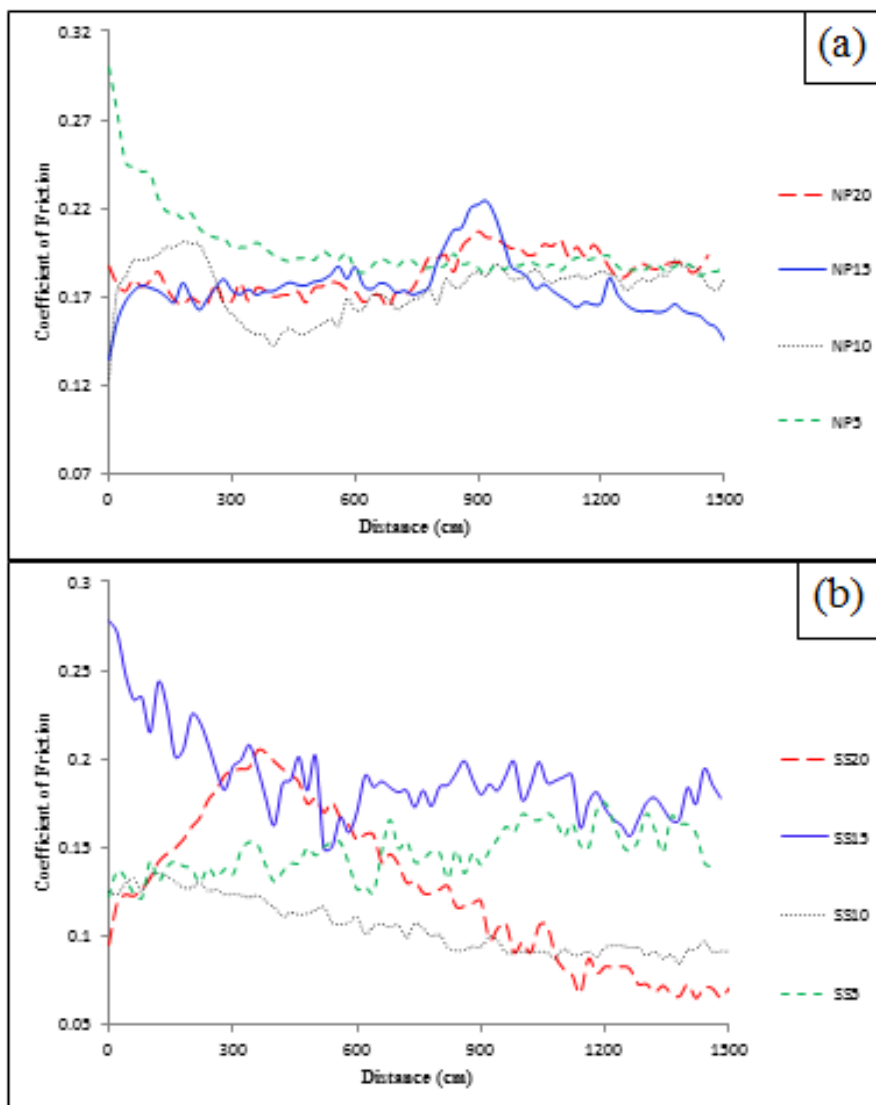


Figure 8. COF variations vs. distance curves of samples resulted from abrading of WC-Co pin on surface of coatings after 1500cm distance: a) coatings with and b) coatings without WC nano-powder.

Table 6. Wear test results: wear rate, wear test width, roughness, hardness and average of COF.

Sample code	Average of Friction Coefficient	Wear Track Width (µm)	Wear Rate (mg/(m.N))×10 ⁻⁴	Hardness (Hv _{0.1})	roughness (R _a)(µm)
NP5	0.20	1291	11.86	464	1.42
NP10	0.18	1638	20.57	390	1.42
NP15	0.18	1358	31.29	650	1.68
NP20	0.18	1458	20.43	326	1.86
SS5	0.15	1819	24.58	295	0.89
SS10	0.11	1713	11.85	296	1.43
SS15	0.19	1896	28.99	271	1.36
SS20	0.13	1888	30.65	265	1.44

Fig. 9 illustrates image and element map of NP15 sample after wear test, and EDS results show good protection of coating. The very low content of Si and Al elements and very high content of Mg inside of wear track shows that the substrate is inchmeal reached due to wear and noticeable amounts of W in this EDS map confirms infiltration of somewhat tungsten into substrate during sparking stage which has been mentioned in section of discussion about EDS from coatings. Here again it can be observed no agglomeration of nano-powders has been occurred during coating process and the coating is worn uniformly.

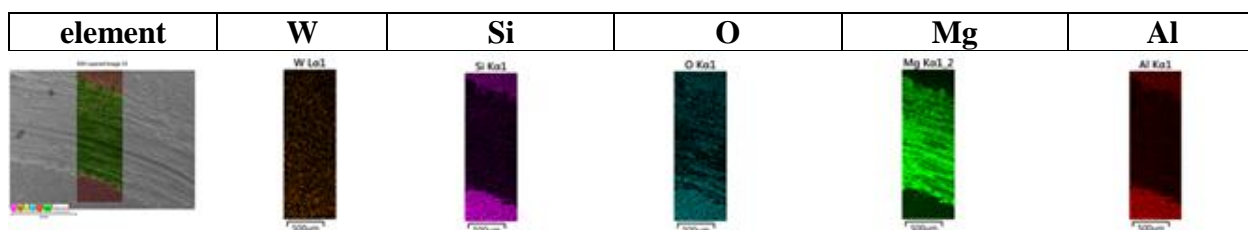


Figure 9. W, Al, Mg, O and Si element distribution map obtained from EDS analysis from wear track of sample NP 15 after wear test. Uniform distribution of W element in the track asserts that no agglomeration occurred during coating process.

4. CONCLUSION

In this article effect of coating time and incorporation of WC nano-particle in nano-composite PEO coatings fabricated on AZ31B Mg alloy is studied. Samples coated in nano-particle suspension had 10 to 17 volts lower sparking potentials. Addition of nano-particles decreased mean pore diameter of coatings from 8.48 to 6.57 μm and average porosity fraction from 18.80% to 12.85 % for coatings without and with nano-powders respectively. There was no agglomeration of nano-powders in structure of coatings. Time pass during coating process in samples containing nano-powders increased nano-powder absorption from 0.99 % to 2.68%. Addition of WC nano-powders to coatings caused only slight improvement in corrosion behavior of samples. Addition of nano-powder increases average COF up to 0.19. Nano-powder presence not only decreases wear track width, but also decreases wear rate from 30.65 to 20.43 $\text{mg}/(\text{m.N})$ for samples without and with nano-powder respectively. Particle agglomeration or oxidation in wear track was not observed. With addition of nano-powder average roughness increases from 1.28 to 1.60 μm for samples without and with nano-powder respectively due to nucleator role of nano-powders.

References

1. D.A. Stewart, P.H. Shipway, and D.G. McCartney, *Wear*, 225 (1999) 789.
2. X. P. Zhang, Z. P. Zhao, F.M. Wu, Y.L. Wang, J. Wu., *J. Mater. Sci.*, 42 (2007) 8523.
3. S. Durdu, A. Aytac, and M. Usta, *J. Alloy Compd.*, 509 (2011) 8601.
4. M. Boinet, S. Verdier, S. Maximovitch, F. Dalard, *Surf. Coat. Tech.*, 199 (2005) 141.
5. L. Chang-Jiu, H. Yang, and H. Li, *Mater. Manuf. Process.*, 14 (1999) 383.

6. B. Li, J. Yao, Q. Zhang, Z. Lia, L. Yanga, *Surf. Coat. Tech.*, 275 (2015) 58.
7. S. Zhang, Q. Li, X. Yang, X. Zhong, Y. Dai, F. Luo, *Mater. Charact.*, 61 (2010) 269.
8. Y. Ma, X. Nie, D.O. Northwood, H. Hu, *Thin Solid Films*, 469 (2004) 472.
9. Y. Ma, X. Nie, D.O. Northwood, H. Hu, *Thin Solid Films*, 494 (2006) 296.
10. H. Duan, C. Yan, F. Wang, *Electrochim. Acta*, 52 (2007) 3785.
11. S. Stojadinović, N. Tadić, N. Radić, B. Stojadinović, B. Grbić, R. Vasilić, *Surf. Coat. Tech.*, 276 (2015) 573.
12. A. Bahramian, K. Raeissi, A. Hakimizad, *Appl. Surf. Sci.*, 351 (2015) 13.
13. Z. Yao, Y. Xu, Y. Liu, D. Wang, Z. Jiang, F. Wang, *J. Alloy Compd.*, 509 (2011) 8469.
14. X. Lu, C. Blawert, M.L. Zheludkevich, K.U. Kainer, *Corros. Sci.*, 101 (2015) 201.
15. S.V. Gnedenkov, S.L. Sinebryukhov, D.V. Mashtalyar, I.M. Imshinetskiy, A.S. Gnedenkov, A.V. Samokhin, Y.V. Tsvetkov, *Vacuum*, 120 (2015) 107.
16. K.M. Lee, K.R. Shin, S. Namgung, B. Yoo, D.H. Shin, *Surf. Coat. Tech.*, 205 (2011) 3779.
17. M. Gheyhani, H. R. Bagheri, H. R. Masiha, M. Aliofkhaezrai, A.S Rouhaghdam, T. Shahrabi, *Surface Eng.*, 30 (2014) 244.
18. S. Stojadinović, N. Tadić, N. Radić, B. Stojadinović, B. Grbić, R. Vasilić, *Surf. Coat. Tech.*, 276 (2015) 573.
19. L. Yu, J. Cao, and Y. Cheng, *Surf. Coat. Tech.*, 276 (2015) 266.
20. E.A. Zen, J. V. Chernosky, *Am. Mineral.*, 61 (1976) 1156.
21. JANAF Thermochemical Tables, 1974 Supplement. *J. Phys. Chem. Ref. Data*, 3 (1974) 311.
22. V.S. Rudnev, M.S. Vasilyeva, N.B. Kondrikov, L.M. Tyrina, *Appl. Surf. Sci.*, 252 (2005) 1211.
23. D. Sreekanth, N. Rameshbabu, and K. Venkateswarlu, *Ceram. Int.*, 38 (2012) 4607.
24. J. Liang, P.B. Srinivasan, C. Blawert, M. Störmer, W. Dietzel, *Electrochim. Acta*, 54 (2009) 3842.
25. W. Zhang, T. Bo, D. Ke-Qin, Z. Hui-Xia, W. Fu-Hui, *Int. J. Electrochem. Sci.*, 6 (2011) 5228.
26. S. Cui, H. Jianmin, D. Yongping, L. Weijing. *Surf. Coat. Tech.*, 201 (2007) 5306.
27. L. Liu, Y. Pei-xia, S. Cai-na, G. Hong-fei, A. Mao-zhong, *Int. J. Electrochem. Sci.*, 8 (2013) 6077.
28. P. Zhang, X. Nie, H. Hu, Y. Liu, *Surf. Coat. Tech.*, 205 (2010) 1508.
29. R.O. Hussein, D.O. Northwood, and X. Nie, *Surf. Coat. Tech.*, 237 (2013) 357.